arXiv:cond-mat/0106561v5 [cond-mat.soft] 12 Apr 2002

Electrophoresis of a Charge-Inverted Macroion Complex: Molecular Dynamics Study

Motohiko Tanaka
National Institute for Fusion Science, Toki 509-5292, Japan

A.Yu.Grosberg
Department of Physics, University of Minnesota, Minneapolis, MN 55455

We have performed molecular dynamics simulations to study the effect of an external electric field on a macroion in the solution of multivalent $Z:1$ salt. To obtain plausible hydrodynamics of the medium, we explicitly make the simulation of many neutral particles along with ions. In a weak electric field, the macroion drifts together with the strongly adsorbed multivalent counterions along the electric field, in the direction proving inversion of the charge sign. The reversed mobility of the macroion is insensitive to the external field, and increases with salt ionic strength. The reversed mobility takes a maximal value at intermediate counterion valence. The motion of the macroion complex does not induce any flow of the neutral solvent away from the macroion, which reveals screening of hydrodynamic interactions at short distances in electrolyte solutions. A very large electric field, comparable to the macroion unscreened field, disrupts charge inversion by stripping the adsorbed counterions off the macroion.

PACS numbers: 61.25.Hq, 82.45.-h, 82.20.Wt

I. INTRODUCTION

The concept of electrostatic screening has been well known since the work by Debye and Hückel of early $20th$ century [1]. In recent years, screening by strongly charged ions was found to result in counterintuitive phenomena such as attraction between like-charged macroions [2, 3, 4, 5], and inversion of macroion charges [6, 7, 8, 9, 10, 11, 12, 13, 14, 15, 16, 17, 18, 19, 20, 21, 22, 23, 24, 25]. Charge inversion was studied by experiments using both colloids and biological materials [6, 7, 8, 9, 10, 11, 12, 13, 14], by analytical theories [16, 18, 19, 20, 21, 24, 25], and by Monte Carlo and molecular dynamics (MD) simulations [15, 17, 22, 23].

Experimentally, the most direct method to observe charged colloids and macroions is electrophoresis. This method is also the prime candidate for the technique of observing charge inversion. Although straightforward, this approach involves many questions upon a closer look. For example, does the macroion drift along with its adsorbed multivalent ions when an external electric field is applied? How many multivalent ions are attached to the macroion strongly enough to drift together? How is the drift affected by the solvent viscosity and the counterflow of monovalent ions? What happens when the field becomes very strong? What is the field strength sufficient to disrupt the charged complex? These are the fundamental questions necessary to address in order to bridge theoretical concepts of charge inversion and experimental observations.

It should be born in mind that electrophoresis in general has quite a few delicate aspects. Some peculiar ones attracted significant attentions recently [26] (see also the review article [27] and references therein). The electric field acts not only on the macroions, but on every ion in a solution. In many cases, this leads to effective screening of hydrodynamic interactions which otherwise may be very significant. In the simulations reported below, we have actually observed such short-range screening of hydrodynamic interactions in the system comprising of a macroion, counterions and coions (Sec.III B 1).

One of the difficulties in simulating charge inversion under electrophoresis consists in subtle interactions of a macroion with surrounding ions and neutral solvent. A naive use of the Langevin equation, assuming that every ion (radius R) in the system is subject to Stokesian friction $-6\pi\eta Rv$ and white noise random forces that balance the friction through the fluctuation-dissipation theorem, is not justifiable. A simple counterexample would be two closely located spheres. Since other particles (either ions or neutral solvent) are excluded from the volume between spheres, neither their corresponding friction forces nor random forces add to each other. One way of going around this problem is to incorporate macroion-solvent interactions using the Oseen tensor [28]. This is, however, not easy to implement in numerical simulations, because the interactions produce complicated spatial correlations among random forces. Therefore, we address this problem by a direct approach introducing explicit neutral particles to deal with the macroion-salt-solvent interactions in the molecular dynamics simulations.

The explicit simulation of the solvent molecules is of course costly. In this paper, with the limited computational resources, we restrict ourselves to the system with only the $Z:1$ salt, and no $1:1$ salt. It is needless to say that in real water solvent there is always some amount of $1:1$ salt. In this sense, our present paper demonstrates the principle that charge inversion is a phenomenon observable by a direct electrophoresis experiment. Further study including the $1:1$ salt will be required to compare results with realistic systems. Here, we will specify the deviations arising from the lack of the $1:1$ salt. Also, we

will confine ourselves to the study of a single macroion interacting with surrounding salt ions and solvent.

Our plan in this study is to examine electrophoresis of a spherically shaped, uniformly charged macroion. We will systematically measure the mobility of the drifting macroion complex placed under an external electric field by molecular dynamics simulations. We first show that charge inversion does take place in a solution containing multivalent counterions, as manifested by the inverse mobility under the weak electric field. We then look at the dependences of the reversed mobility on the parameters, such as the concentration of co- and counterions and the surface charge density of the macroion. Finally, we consider the strong electric field regime and show that the strong field disrupts the charge-inverted macroion complex and terminates the charge inversion phenomenon.

II. SIMULATION MODEL AND PARAMETERS

A. Description of the Model

We adopt the following model, with a, e, and m being the units of length, charge and mass, respectively. (We have in mind $a \sim 2$Å and $m \sim 40$ a.m.u.) A macroion with negative charge Q_0 between $-15e$ and $-180e$ is surrounded by N^+ counterions of a positive charge Ze and $N^- \approx 300$ coions of a negative charge $-e$. The system is maintained in overall charge neutrality, $Q_0 + N^+Ze - N^-e = 0$, which determines N^+ for a given Z. The mass of the macroion is $M = 200m$, and the mass of the co- and counter-ions is m. We also include N_* neutral particles with mass $m/2$, where we note the mass of water molecule against that of K^+ or Ca^{2+} ions. Approximately one neutral particle is located in every volume element $(1.5a)^3 \approx (3\text{Å})^3$ inside the simulation domain, excluding the locations already occupied by the macroion and other ions, which typically yields 8000 neutral particles. These particles are confined in a rectangular box of size L, with periodic boundary conditions in all three directions. Most of the runs are performed for $L = 32a$, except one series of the runs intended to test the finite size effect of the domain (Fig.4) described in Sec.III B 1.

In addition to the Coulomb forces, all particles interact through the repulsive Lennard-Jones potential $\phi_{LJ} = 4\varepsilon[(\sigma/r_{ij})^{12} - (\sigma/r_{ij})^6]$ for $r_{ij} = |\mathbf{r}_i - \mathbf{r}_j| \le 2^{1/6}\sigma$, and $\phi_{LJ} = -\varepsilon$ otherwise. Here $\mathbf{r}_i$ is the position vector of the i-th particle, and σ is the sum of the radii of two interacting particles, which are chosen as follows: radius of the macroion, R_0, is between $3a$ and $5a$, counterions and coions have radius a, and neutral particles $a/2$. We relate ε with the temperature by $\varepsilon = k_BT$, and choose $k_BT = e^2/5\epsilon a$ (we assume spatially homogeneous dielectric constant ϵ). The Bjerrum length is thus $\lambda_B = e^2/\epsilon k_BT = 5a$. For the parameters of this temperature, the valence $Z = 3$, and the number of coions $N^- = 300$, the ionic strength becomes $n_I = (Z^2N^+ + N^-)/L^3 \sim 3.7 \times 10^{-2}a^{-3}$.

After knowing the ionic strength, one is tempted to compute the Debye length which turns out to be $\lambda_D \sim 0.45a$. We should emphasize that this number does not have much meaning for the system under study, because we work in the domain very far from applicability of the standard Debye-Hückel theory. In particular, the average number of ions in the volume λ_D^3 turns out smaller than unity. This is by no means surprising, because there is no charge inversion in the Debye-Hückel theory, and to examine charge inversion we need to go to the regime where this theory fails.

Since we do not have the $1:1$ salt in our simulation, we should keep in mind that correlations between strongly charged Z-ions may be significant even away from the macroion. Indeed, in the theory of charge inversion [19], the role of correlations is emphasized for the Z-ions in the vicinity of the macroion, where their concentration is particularly large. In our system, the concentration of the Z-ions is not very small even in the bulk, and we face the situations in which correlations between the Z-ions away from the macroion affect our results. For such cases, we make additional runs with the reduced concentration in the $Z:1$ salt. However, we do not use this reduced concentration for all the runs, because such system is more prone to noises and fluctuations, requiring larger statistics to obtain reliable results.

Calculation of the Coulomb forces under the periodic boundary conditions involves the charge sum in the first Brillouin zone and their infinite mirror images (the Ewald sum[29]). The sum is calculated with the use of the PPPM algorithm [30, 31]. We use $(32)^3$ spatial meshes for the calculation of the reciprocal space contributions to the Coulomb forces, with the Ewald parameter $\alpha \approx 0.262$ and the real-space cutoff $r_{cut} = R_i + 10a$, where R_i is the radius of the i-th ion. A uniform electric field E is applied in the x-direction.

When starting the molecular dynamics simulation run, we prepare an initial state by randomly positioning all the ions and neutral particles in the simulation domain and giving Maxwell-distributed random velocities corresponding to the temperature T_{initial}. We integrate the Newton equations of motion with the use of the leapfrog method [32], which is equivalent to the Verlet algorithm. In the absence of the electric field ($E = 0$), our system is closed, and its energy is conserved. After an initial transient phase, the distribution of velocities relaxes to a Maxwellian, corresponding to an equilibrium sampling of the microcanonical ensemble. This new Maxwell distribution has the temperature T, which is a little higher than T_{initial}, because of the release of the potential energy due to screening, i.e., local balancing of charges. We adjust T_{initial} such that $k_BT = \varepsilon$. This makes ε to be the unique relevant scale of energy, and, accordingly, we put $\tau = a\sqrt{m/\varepsilon}$ as the unit of time. We choose $\Delta t = 0.01\tau$ as the integration time step. The simulation runs are executed up to 1000τ.

B. Hydrodynamic interactions, their screening, and the temperature control

When an external electric field is present, it performs work on the system. The corresponding energy, which is the Joule heat, is transferred to background neutral particles through collisions with accelerated ions. In our work, we simulate an electrophoretic bath that is kept at a constant temperature T. For this purpose, we pretend that all neutral particles go through the thermal bath of infinite heat capacitance, whenever they cross the boundaries of the simulation domain (at the center of which the macroion is located at every moment). Operationally, we refresh the velocities of the neutral particles according to the thermal distribution when they cross the domain boundaries. This procedure maintains temperature stably to within 5%.

Two closely related factors are potentially dangerous as they might affect the molecular dynamics simulation results. One factor is the finite-size of the simulation domain, and the other is the long-range character of both hydrodynamic and Coulomb interactions. These problems become particularly important because some of the methods to simulate a constant temperature thermal bath are believed to lead to the screening of hydrodynamic interactions. This is obviously not acceptable in the simulation where the long range character of hydrodynamic interactions is expected to be important [33].

Following [26, 27], we argue that hydrodynamic interactions are in fact effectively screened in our system and, therefore, that the domain size in our simulation is quite sufficient and the heat bath procedure described above is benign and reliable.

To understand the situation, it is worth discussing the major point - the screening of hydrodynamic interactions. To begin with, why are hydrodynamic interactions long ranged? That fact can be understood well from the point of view of momentum conservation. Consider a particle immersed in a fluid and suppose that we pull this particle with an externally applied force (such as gravity). Obviously, this force transfers momentum into the system and, however large the container may be, this momentum must be transported away through the container walls. This necessitates the long range character of the hydrodynamic field. More accurately, if we surround our object by an arbitrarily large closed surface, then (under the stationary conditions) the outflow of momentum through this surface must be equal to the inflow of momentum due to the external force. Because of the obvious analogy with the Gauss theorem in electrostatics, we see that hydrodynamic field is just as long ranged as the Coulomb field (even though it has a more complicated vector structure).

The above description must be modified significantly when the applied external force is due to the electric field and the solution is neutral as a whole. In this case, there is no overall inflow of momentum into the system, and therefore, there should not be any outflow through the walls of the container. More specifically, if there is one negatively charged macroion as in our simulation, it is surrounded by positively charged counterions and negatively charged coions such that the total charge of the crowd effectively vanishes at some finite distance. In the simple case of the Debye-Hückel theory, this happens at about the Debye screening length λ_D from the macroion surface. Therefore, no momentum is transported further away, and hydrodynamic interactions are screened at the distances of the order of λ_D [26, 27].

In this paper, we treat a more complicated situation in which the Debye-Hückel theory does not apply and it is not easy to judge *a priori* at which distances the hydrodynamic interactions are screened. Nevertheless, since the system is neutral, hydrodynamic interactions must be screened. We therefore perform special test (described in Sec.III B 1) looking at the dependence of the macroion drift on the simulation domain size. We find that the drift is essentially size-independent at $L > 20a$ which is the direct manifestation of the screening of hydrodynamic interactions.

Since hydrodynamic interactions are screened, our simulation is not very sensitive to the method of maintaining the constant temperature. To test it, we have performed separate runs at weak electric fields, $E \leq 0.3\varepsilon/ae$, in which case we can run the simulation even without any heat drainage for a significant period of time before any noticeable heating of the system; the results of these control runs are within error bars of the data obtained using the thermal bath (Fig.5).

III. SIMULATION RESULTS

A. General Properties

Our simulation results are shown in Figs.1-7. Fig. 1 is a bird's-eye view of (a) all the ions and (b) the vicinity of the macroion. Counterions are shown in light blue and coions in dark blue (neutral atoms are not shown). In this figure, the macroion charge is taken to be $Q_0 = -30e$, its radius $R_0 = 3a$, counterion valence $Z = 3$, and the electric field $E = 0.3\varepsilon/ea$. It is seen that the macroion is predominantly covered by the counterions. As in the case without the electric field [23], the radially integrated charge has a sharp positive peak at a distance about a from the macroion surface. This peak is due to the positive counterions being adsorbed on the macroion surface. The value of the peak charge under the conditions of Fig.1 is $Q_{\rm peak} \approx 1.6|Q_0|$.

Fig. 2 demonstrates the time history of (a) the "peak" charge and (b) the macroion drift speed for the parameters of Fig.1. At time $t = 10\tau$, we switch on the external electric field. There is a short transient phase during which a charge-inverted complex is formed through adsorption of counterions to the macroion and condensation of coions on the counterions. This process is reflected in a rather quick rise in $Q_{\rm peak}$, as is shown in Fig.2(a). After the transient phase, we observe a drift of the macroion

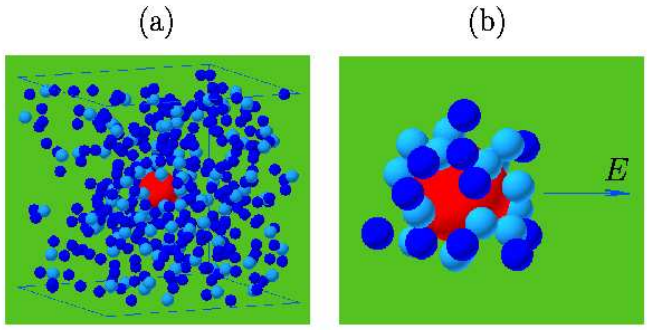

FIG. 1: Bird's-eye view of (a) all the ions in the simulation domain and (b) the screening ion atmosphere within $3a$ from the macroion surface. A macroion with charge $Q_0 = -30e$ and radius $R_0 = 3a$ is a large sphere in the middle; counterions ($Z = 3$) and monovalent coions are shown by light and dark blue spheres, respectively. The arrow to the right shows the direction of the electric field (x-axis), with $E = 0.3\varepsilon/ea$.

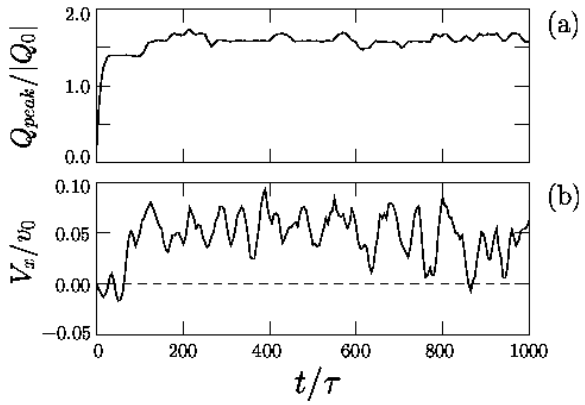

FIG. 2: Time history of (a) the *peak* charge Q_{peak} (defined as the maximum of radial charge distribution around the macroion center) and (b) the macroion speed V_x normalized by thermal velocity of neutral particles v_0. The macroion complex drifts positively along the external electric field of $E > 0$, which directly indicates the inversion of the charge sign.

in the *positive* direction along the applied field. The fact that the drift velocity is positive for the negative bare charge of the macroion ($Q_0 < 0$) is a direct manifestation of charge inversion such that counterions are so strongly bound that they pull the macroion with their motion.

Note that the drift velocity shown in Fig.2(b) is small compared to the thermal velocity v_0 of neutral particles, $\langle V_x \rangle \sim 0.05 v_0$. Under this condition, exchange of momentum between the macroion and neutral particles is slow, and it requires many collisions (compare the similar system in Ref.[34]). Therefore, in terms of hydrodynamics, we are in the linear regime. It means that friction force should be linear in the macroion velocity and we expect the average drift speed to be given by the force balance condition, $Q^*E - \nu V_x = 0$, where Q^* is the effective net charge of the macroion complex and ν is the hydrodynamic friction coefficient. We shall discuss later the possibilities of determination of the effective net charge Q^* based on this condition.

Fig. 2 also shows significant temporal fluctuations in the drift speed. Inspection reveals that they are larger than what one expects for random kicks of neutral particles. These fluctuations indicate that neither the counterions permanently stick to fixed points on the macroion nor the coions attach to the counterions, but that they are being replaced from time to time. The fluctuations of this type are actually seen in a video movie.

B. Parameter Dependences

1. *Linear Regime*

The dependence of the average macroion drift speed $V_{\rm drift}$ on the electric field is shown in Fig.3. In this figure, we show together the results of several runs, corresponding to different values of the macroion charge Q_0 and macroion radius R_0. First and foremost, the sign of the drift velocity in moderate fields corresponds to the sign of inverted charge. This is the central observation of our work. The figure clearly demonstrates the overall pattern of the drift velocity dependence on the applied field, beginning with the linear regime in a weak field, followed eventually by a breakdown of charge inversion in a strong field.

Let us discuss the linear drift regime for small electric fields $E \leq 0.2|Q_0|/\epsilon R_0^2$, where $V_{\rm drift}$ increases linearly with the field strength. This regime corresponds to the usual Ohm's law, where the net charge of the complex is insensitive to the strength of the electric field. A macroion drifts together with its strongly adsorbed counterions as a complex. That is, the electric field is not strong enough to affect the binding of counterions to the macroion.

At this stage, it is necessary to check the issue of hydrodynamic interactions and their screening. For that purpose, we show in Fig. 4 the effect of the simulation domain size L on the macroion drift speed. By a series of the runs with different domain sizes and under fixed number density of neutral particles and ionic strength, we have confirmed that at $L = 32a$, which is the domain size for the majority of our simulations, the domain-size dependence is essentially leveled off. This is to be contrasted with polymer chains [33], in which case hydrodynamic interactions lead to the finite size effect essentially linear in a/L.

We have also inspected the fluid flow of neutral particles around the macroion. When rapid fluctuations are averaged out, this flow field does not exhibit any patterns protruding away from the macroion. This fact implies that the flow of neutral particles induced by the motion of the macroion and other ions is screened at short distances [26, 27].

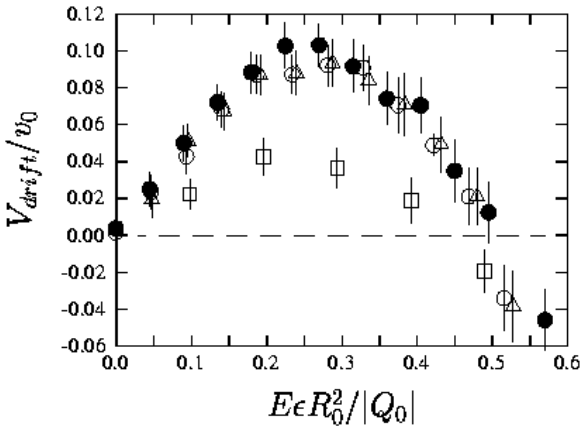

FIG. 3: Dependence of the macroion drift speed $V_{\rm drift}$ (in the units of v_0, the thermal speed of neutral particles) on the electric field E for a macroion of various radii and charges: $R_0 = 3a$ and $Q_0 = -30e$ (filled circles); $R_0 = 4a$ and $Q_0 = -50e$ (open triangles); and $R_0 = 5a$ and $Q_0 = -80e$ (open circles); $R_0 = 5a$ and $Q_0 = -51e$ (open squares). The valence of counterions is $Z = 3$.

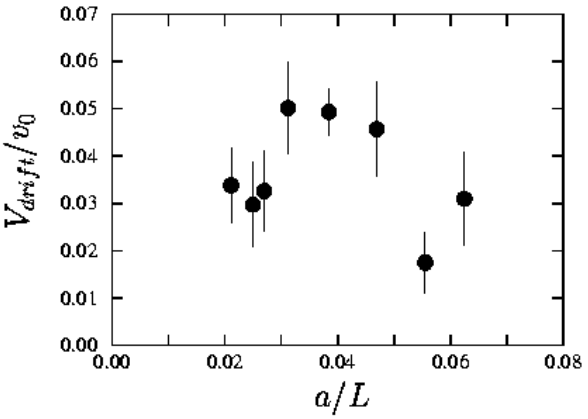

FIG. 4: Effect of the finite domain size L on the drift speed V_{drift} for a macroion with $R_0 = 3a$, $Q_0 = -30e$, the electric field $E = 0.3\varepsilon/ae$, and counterion valence $Z = 3$. The error bars correspond to the root mean square velocity fluctuations as seen in Fig. 2.

The saturation of the a/L dependence (Fig. 4) and the inspection of neutral particle flow patterns both confirm that hydrodynamic interactions are screened in our system, thus making reliable our simulation approach based on the finite domain and the heat bath. The thermal bath at the distant boundaries does not affect the measured macroion mobility.

The small electric field regime is characterized by the mobility, $\mu = \langle V_x \rangle / E$. This quantity is plotted in Fig. 5 as a function of the macroion bare charge Q_0, or, more specifically, on the surface charge density of the macroion $|Q_0|/R_0^2$.

2. *Can we measure net charge based on the mobility measurement data?*

Let us now discuss a practically important question: Can we determine the effective net charge of the macroion complex Q^* based on the data of mobility measurements, i.e., based on the data of Fig.5 - Fig.7 ? Physically, as we have already mentioned, the charge Q^* is determined by the force balance condition $Q^*E - \nu V_x = 0$, or $Q^* = \mu\nu$. Therefore, determination of the net charge requires knowledge of both the friction coefficient ν and the mobility μ.

Importantly, the friction coefficient cannot be determined by the usual Stokes formula $\nu_S = 6\pi\eta R$, where η is the solvent viscosity. The problem is that the real friction is enhanced by the screening of hydrodynamic interactions [26, 27]. The Stokes formula is simply understood by that the friction force in general should be proportional to $\eta(v/A)B^2$, where A is the length scale over which velocity changes, B^2 is the relevant surface area. For the Stokes problem, we have $A \sim B \sim R_0$. By contrast, when the drift is caused by the action of the electric field on the overall neutral system, the distance A becomes much smaller. In the Debye-Hückel theory, it turns out to be of the order of the Debye screening length, $A \sim \lambda_D$. In this case, the friction coefficient becomes

$$\nu = \nu_S R_0/\lambda_D \ , \qquad (1)$$

i.e., it is enhanced by the factor R_0/λ_D compared to the usual Stokesian friction. Although we work under the conditions where the Debye-Hückel theory is not applicable, and we do not know exactly which length should be there instead of λ_D in Eq.(1), this length is clearly smaller than R_0 and independent of R_0. Therefore, the friction coefficient is proportional to R_0^2 - unlike more familiar Stokes case where it scales like R_0.

Under usual circumstances where the charge Q^* is known, the friction coefficient scaling as R_0^2 implies that mobility $\mu = Q^*/\nu \propto Q^*/R_0^2$ is determined by the *surface charge density*, not by the charge and the surface area separately. This fact was known to M.Smoluchowski already a century ago [35]. In our simulation, effective charge is not known *a priori*, and the logic needs to be reversed. Figure 5 indicates that mobility μ is essentially a constant when the macroion bare surface charge density is not too small ($|Q_0|a^2/eR_0^2 \geq 3$). Given that $\nu \propto R_0^2$, we conclude that the effective bare charge $Q^* = \mu\nu$ is proportional to the surface area of the macroion; namely, charge inversion is characterized by the overcharging density. This agrees with the theory [20, 25].

In order to perform at least very rough quantitative estimate of charge Q^* based on the mobility data, we need to know the Stokesian friction coefficient ν_S (or equivalently, we need to know the viscosity of our model solvent). We measure it in a separate molecular dynamics run, by observing an exponential decay of the macroion velocity starting from $0.5v_0$ for the case without an electric field. We find $\nu_S \approx 9.3m/\tau$ for a spherical particle of

the radius $R_0 = 3a$ and $\nu_S \approx 18.2m/\tau$ for the macroion complex with adsorbed counterions and coions. These two estimates provide lower and upper bounds for the charge Q^*. Assuming $R_0/\lambda_D \approx 6$ and $\mu \approx 0.5\mu_0$ (saturation regime in Fig.5) yields the inverted charge Q^* between $7e$ and $20e$. This is in rough agreement with the Q_{peak} measurements.

Special attention must be paid to the small bare surface charge density case, for which Fig.5 indicates the decrease in the reversed mobility. For some cases, the reversed mobility even disappears altogether, changing to normal, non-reversed mobility, $\mu < 0$ when the macroion bare surface charge density decreases to about $|Q_0|a^2/eR_0^2 \sim 1$. It turns out that this is the manifestation of correlations between Z-ions in the bulk solution away from the macroion. Indeed, when the macroion is only weakly charged, the correlations of Z-ions in its vicinity are not much stronger than in the bulk, which suppresses charge inversion. Simple estimate shows that, under the conditions when μ gets small or negative in Fig.5, the "Wigner cell" radius of the Z-ions on the macroion surface, $R_W = 2R_0(eZ/|Q_0|)^{1/2}$ (which is about $3.4a$ for $|Q_0|a^2/eR_0^2 \approx 1$ and $Z = 3$) becomes comparable to the average spacing between the Z-ions in the bulk. The inspection of the radial charge distribution functions around the macroion for this case agrees with this interpretation. It shows that the counterions are loosely bound to the macroion, and that the coions form relatively strong bonds with the counterions and drift together with them.

To examine the above interpretation further, we perform special runs with reduced concentration of the $Z:1$ salt. The results of these runs are shown in Fig.5 with filled circles and triangles for the $N^+ = (N^-e + |Q_0|)/Ze$ Z-ions with $N^- = 90$ and 30 negative coions, respectively. As anticipated, with fewer Z-ions in the bulk, charge inversion is not interrupted even at small macroion bare charges. We regard this a convincing proof that charge inversion occurs at small concentration of the Z-ions *despite* a larger entropy penalty.

Figure 5 also shows with crosses the data of the control run performed under the condition of the weak electric field without any heat drainage (see Sec.II B). These data are within error bars of the cases with the simulated thermal bath.

The dependence of the macroion mobility μ on the valence of the counterions Z in Fig.6 is physically interesting, and also important for application purposes. For the cases shown with filled and open circles, the surface charge density of the macroion is chosen nearly the same $|Q_0|/R_0^2 \sim 3$ so that they reside in the saturation regime of Fig.5. We emphasize that the mobility for these cases is given by the same curve. The mobility of the macroion is *negative* when counterions are monovalent $Z = 1$, because there is no charge inversion but only regular Debye screening. Thus, the charge inversion phenomenon does not occur in the solution of monovalent salt (provided that the co- and counter-ions have the equal radius). For

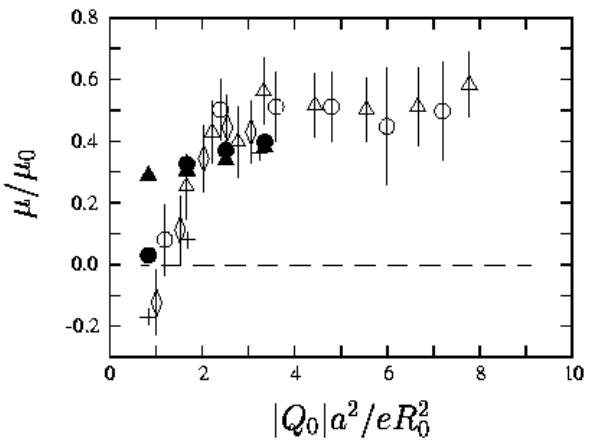

FIG. 5: Dependence of the macroion mobility μ on the surface charge density Q_0/R_0^2 for the macroion radius $R_0 = 3a$ (open triangles), $R_0 = 5a$ (open circles), and $R_0 = 7a$ (open diamonds), where $\mu_0 = v_0/(|Q_0^{(0)}|/\epsilon(R_0^{(0)})^2)$ with $Q_0^{(0)} = -30e$ and $R_0^{(0)} = 3a$. The valence of the counterions is $Z = 3$, the number of the $Z:1$ salt is $N^+ = (N^-e + |Q_0|)/Ze$ and $N^- = 300$, the electric field is $E = 0.3\varepsilon/ae$, and the temperature is $e^2/\epsilon ak_BT = 5$. The filled circles and triangles show the cases with reduced number of the $Z:1$ salt such that $N^- = 90$ and 30, respectively. The crosses are the reference data obtained without the thermal bath for $R_0 = 5a$ and the $Z:1$ salt with $N^- = 300$.

$Z \geq 2$, charge inversion does take place, as manifested by the *positive* mobility. These observations agree with a previous study for planar charged surfaces [18]. A remarkable finding is that the mobility here is maximized for the intermediate valence, $Z \approx 4$, unlike the peak inverted charge that accounts for static charge distribution of mainly counterions [23].

It is also noted in Fig.6 that, when the surface charge density is reduced, both the magnitude of reversed (positive) mobility and the range of Z where it occurs shrink as shown by square symbols in the figure. The mobility for divalent Z-ions is now negative. This corresponds to the small surface charge density regime $|Q_0|/R_0^2 \sim 1.6$ in Fig.5. Yet, the mobility is maximized for the intermediate valence, $Z \cong 5$ in this case. Also shown in Fig.6 are the results of the control runs performed with reduced number of Z-ions (discussed above in connection with Fig. 5). They again reproduce the optimal valences for charge inversion.

Although somewhat speculative, we can try to apply the result of Fig.6 to explain the electrophoretic mobility measurements of nucleosome core particles in cation solution [14]. What was observed is the increase in the magnitude and range of the cation concentration for occurrence of reversed mobility when spermidine salt (+3) was replaced with spermine salt (+4), while charge reversal was not observed for any concentration of Mg^{+2}. It is worth stressing that nucleosome particles is a complicated system in which many aspects may be important.

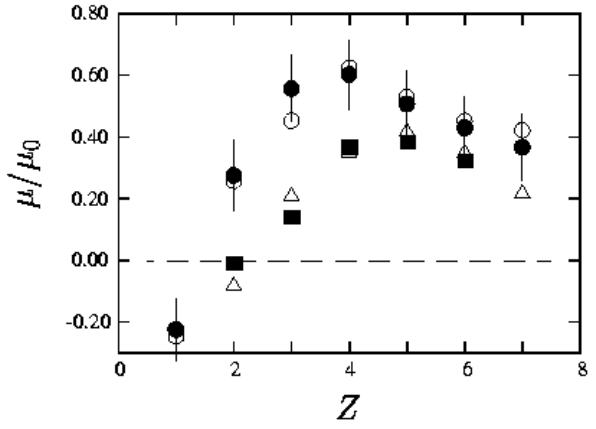

FIG. 6: Dependence of the macroion mobility μ on the valence of the counterions Z for the runs: $R_0 = 3a$ and $Q_0 = -30e$ (filled circles), $R_0 = 5a$ and $Q_0 = -80e$ (open circles), and $R_0 = 5a$ and $Q_0 = -40e$ (filled squares). Here, the number of the $Z:1$ salt is $N^+ = (N^-e + |Q_0|)/Ze$ and $N^- \approx 300$, the external electric field is $E = 0.3\varepsilon/ae$, where $\mu_0 = v_0/(|Q_0^{(0)}|/\epsilon(R_0^{(0)})^2$ with $Q_0^{(0)} = -30e$ and $R_0^{(0)} = 3a$. A series of the runs with reduced number of the $Z:1$ salt $N^- \approx 30$, $R_0 = 5a$, and $Q_0 = -80e$ are shown with open triangles.

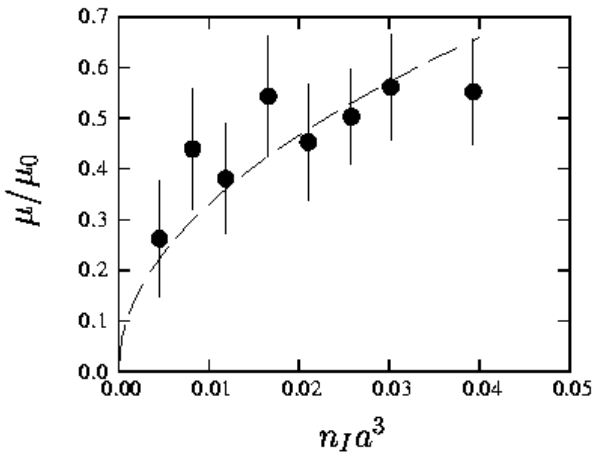

FIG. 7: Dependence of the macroion mobility μ on the salt ionic strength, $n_I = (Z^2N^+ + N^-)/L^3$. The parameters are $Q_0 = -30e$, $R_0 = 3a$, $E = 0.3\varepsilon/ae$, $Z = 3$ and $e^2/\epsilon ak_BT = 5$, which yield the Debye length $\lambda_D \sim 0.45a$ for $n_I = 0.04a^{-3}$.

What we would like to say here is that our results may be at least one of the factors relevant to the experiments reported in the literature [14].

The dependence of the macroion mobility on the salt ionic strength, $n_I = (Z^2N^+ + N^-)/L^3$ is shown in Fig.7 for the counterion valence $Z = 3$ and the temperature $e^2/\epsilon ak_BT = 5$. Here, the ionic strength is related to the Debye length by $\lambda_D = (\epsilon k_BT/8\pi n_I e^2)^{1/2}$. The mobility increases quite rapidly for small ionic strength, and is well fit by $\mu \propto n_I^{1/2}$ as shown by a dashed curve.

It is a legitimate concern to ask whether the data of Fig.7 are affected by the correlations of Z-ions in the bulk which we discussed in connection with Fig. 5. The answer is negative; these data correspond to the saturation regime of Fig. 5. The distance between Z-ions in the bulk drops to the value comparable to the Wigner-Seitz cell only when n_Ia^3 gets as large as 0.1 or more.

The increase in the mobility with ionic strength contradicts the intuition based on the Debye-Hückel theory, and deserves a comment. As it is explained in detail in [25] and understood by a number of authors cited there, charge inversion itself grows with ionic strength. This happens because charge inversion is the result of interplay between the repulsion of counterions from each other and the attraction of each of them to its own correlation hole. The latter occurs at a much shorter distance than the former, and only the repulsion is strongly affected by screening. This is why the amount of charge inversion, hence the macroion mobility, grows with increasing ionic strength.

It is also worth mentioning that the quick rise in the reversed mobility at small ionic strength in Fig.7 agrees with the colloidal mobility measurement for the case with trivalent salt $LaCl_3$ [8, 16].

3. Nonlinear Regime

Let us now return to Fig.3 to discuss the regime that is nonlinear in the applied electric field. As the figure indicates, the charge-inverted shell around the macroion is destroyed for large electric fields. Moreover, the critical field E_c at which this happens is independent of the macroion size, which leads us to an estimate

$$E_c \approx 0.5|Q_0|/\epsilon R_0^2 \ . \qquad (2)$$

This result is quite interesting. Indeed, $|Q_0|/\epsilon R_0^2$ is the electric field on the macroion surface produced by the macroion bare charge. Why does the critical field scale with the bare charge of the macroion instead of the net charge of the complex ? The reason is due to correlations between screening ions. We noted while discussing Fig.2 that the counterions on the macroion surface are being replaced from time to time. Consider how one Z-ion can depart from the macroion surface. Since this ion is surrounded by a correlation hole on the surface, its departure requires work against the unscreened bare electric field of the macroion as long as its distance from the surface is smaller than the distance between the adsorbed Z-ions. Therefore, departure from the surface becomes possible when the external field becomes comparable with this unscreened field; the charge-inverted complex is no longer stable at such a field strength.

The critical electric field in realistic situations is estimated to be very large. For the parameters $R_0 \approx 20$Åand $Q_0 \approx 30e$, the critical electric field becomes as large as $E_c \approx 0.5Q_0/\epsilon R_0^2 \approx 67V/\mu m$, where we take into account

the dielectric constant of water $\epsilon \approx 80$ [36]. Although the critical field is large, it gives small energy to the electric dipole of a water molecule, $d \approx 2 \times 10^{-18}$esu $\cdot$ cm: $E_c d/k_B T \sim 0.11 < 1$. This verifies the use of the model solvent of neutral particles in the present molecular dynamics simulations. In practice, the applied electric field is not expected to disrupt the charge-inverted macroion complex.

IV. SUMMARY

In this paper, we performed molecular dynamics simulations with the use of neutral-particle solvent, and measured the drift speed of a macroion to obtain its mobility under electrophoresis in a multivalent $Z:1$ salt solution.

A weak electric field pulled the macroion complex in the direction determined by the net inverted charge, instead of disrupting it. The reversed mobility of the complex, $\mu = V_{drift}/E$, was shown to be nearly constant for the weak electric fields. We showed the functional dependences of mobility in Figs.3, 5 and 6 of Sec.III, respectively, against the electric field strength E, the surface charge density of the macroion Q_0/R_0^2, and the valence Z of the counterions. The mobility was a function of the surface charge density, instead of the bare charge and radius of the macroion separately. The reversed mobility increased rapidly with the salt ionic strength n_I as $\mu \propto n_I^{1/2}$. Interestingly, the reversed mobility took a maximal value at the intermediate valence of the counterions $Z \cong 4$.

We confirmed the screening of hydrodynamic interactions at a few Debye length. No specific flow patterns of neutral particles, which one would expect for the sphere moving in a viscous fluid, were detected around a macroion.

In the large field regime, although academic because of its huge value, electrophoresis was strongly nonlinear, and the field stripped the screening counterions off the macroion. The mobility of the macroion complex dropped significantly from that of the linear regime, and the sign of the mobility flipped back to non-reversed one above the critical electric field, which was approximately half the macroion *unscreened* field.

In this study, we explicitly simulated the neutral particles of the solvent to produce a reliable hydrodynamic background. On the other hand, the limits of computational resources prevented us from inclusion of the $1:1$ salt. The screening in our system was exclusively accomplished by the $Z:1$ salt. For this reason, we are not ready to make a quantitative comparison of our data with the real experiments. The simulation including the $1:1$ salt is currently under way.

The authors are grateful to Professor B.Shklovskii and Dr.T. Nguyen for discussions, and to Dr.J.W.Van Dam for reading the manuscript. One of the authors (M.T.) thanks Professor K.Kremer and Dr.C.Holm for collaboration on the PPPM algorithm during his stay at the Max-Planck Institut für Polymerforschung (Mainz, 1999) under the support of the Max-Planck Society. The numerical computation was performed with the vpp800/13 of the Institute of Space and Astronautical Science (Japan), and partly with the Origin 3800 of the University of Minnesota Supercomputing Institute.

[1] P. Debye and E. Hückel, *Phys.Zeitsch.* **24**, (1923) 185.
[2] J.C.Crocker and D.G.Grier, *Phys.Rev.Lett.* **73**, (1994) 352.
[3] I. Rouzina and V. A. Bloomfield, *J.Phys.Chem.* **100**, (1996) 9977.
[4] P.Linse and V.Lobaskin, *Phys.Rev.Lett.* **83**, (1999) 4208.
[5] T.Squires and M.Brenner, *Phys.Rev.Lett.* **85**, (2000) 4976.
[6] H.G. Bungenberg de Jong, *Colloid Science, vol.2*, edited by H.R. Kruyt (Elsevier, 1949) 259-330.
[7] U.P.Strauss, N.L.Gershfeld, and H.Spiera, *J.Amer. Chem. Soc.* **76**, (1954) 5909.
[8] M.Elimelch, and C.R.O'Melia, *Colloids Surf.* **44**, (1990) 165.
[9] J.Xia and P. L. Dubin, *Macromolecular complexes in Chemistry and Biology*, edited by P.L.Dubin et al. (Springer-Verlag, Berlin, 1994).
[10] A.V.Kabanov, and V.A.Kabanov, *Bioconjug. Chem.* **6**, (1995) 7.
[11] H.W. Walker and S.B. Grant, *Colloids and Surfaces A* **119**, (1996) 229.
[12] A.V.Kabanov, and V.A.Kabanov, *Advanced Drug Delivery Reviews* **30**, (1998) 49.
[13] H.M. Evans, A. Ahmad, T. Pfohl, A. Martin and C.R. Safinya, *Bull.APS* **46**, (2001) 391.
[14] M.de Frutos, E.Raspaud, A.Leforestier, and F.Livolant, *Biophys.J.* **81**, (2001) 1127.
[15] W.van Mengen, and I.Snook, *J.Chem.Phys.* **73**, (1980) 4656.
[16] E.Gonzales-Tovar, M.Lozada-Cassou, and D.J. Henderson, *J. Chem.Phys.* **83**, (1985) 361.
[17] L.Sjostrom, T.Akesson and B.Jonsson, *Ber.Bunsenges. Phys.Chem.* **100**, (1996) 889.
[18] H.Greberg, and R.Kjellander, *J.Chem.Phys.* **108**, (1998) 2940.
[19] B.I.Shklovskii, *Phys.Rev.E* **60**, (1999) 5802.
[20] T.T.Nguyen, A.Yu. Grosberg and B.I. Shklovskii, *Phys. Rev. Lett.* **85**, (2000) 1568.
[21] F.J.Solis, and M.Olvera de la Cruz, *J.Chem.Phys.* **112**, (2000) 2030.
[22] R.Messina, C.Holm and K.Kremer, *Phys.Rev.Lett.* **85**, (2000) 872.
[23] M.Tanaka and A.Yu. Grosberg, *J.Chem.Phys.* **115**, (2001) 567.
[24] M.Lozada-Cassou, E.Gonzales-Tovar, and W.Olivares, *Phys.Rev. E 60*, (1999) R17; M.Lozada-Cassou and E.Gonzales-Tovar, *J.Colloid Interf.Sci.* **239**, (2001) 285.
[25] A.Yu. Grosberg. T.T. Nguyen, and B.I. Shklovskii,

Rev.Mod.Phys., **74**, (2002).
[26] D.Long, J.-L.Viovy, and A.Ajdari, *Phys.Rev.Lett.* **76**, (1996) 3858.
[27] J.-L.Viovy, *Rev.Mod.Phys.* **72**, (2000) 813.
[28] L.D. Landau and E.M. Lifshitz, *Theoretical Physics, vol. 6, Fluid Mechanics* (Butterworth-Heinemann, 1990).
[29] P.P.Ewald, *Ann.Physik* **64**, (1921) 253.
[30] J.W.Eastwood and R.W.Hockney, *J.Comput.Phys.* **16**, (1974) 342.
[31] M.Deserno and C.Holm, *J.Chem.Phys.* **109**, (1998) 7678.
[32] D.Frenkel and B.Smit, *Understanding Molecular Simulation* (Academic Press, 1996)
[33] B.Dünweg, *J.Chem.Phys.* **99** (1993) 6977.
[34] E.M.Lifshitz and L.P.Pitaevskii, *Theoretical Physics, vol. 10, Physical Kinetics* (Butterworth-Heinemann, 1981), Chapter 2.
[35] M.Smoluchowski, *Bull. International de l'Academie des Sciences de Cracovie* **8**, (1903) 182-200.
[36] I.Ohmine and S.Saito, *Accounts Chem. Res.* **32**, (1999) 741.